ELSEVIER

Engineering Analysis with Boundary Elements xx (0000) xxx–xxx

ENGINEERING ANALYSIS *with* BOUNDARY ELEMENTS

www.elsevier.com/locate/enganabound

An implicit and explicit BEM sensitivity approach for thermo-structural optimization

Thomas J. Martin[a,*], George S. Dulikravich[b,1]

[a]*Pratt and Whitney Engine Co., 400 Main St., MS 165-16, East Hartford, CT 06108, USA*

[b]*Department of Mechanical and Aerospace Engineering, UTA Box 19018, The University of Texas at Arlington, Arlington, TX 76019, USA*

Received 6 February 2002; revised 8 June 2002; accepted 17 June 2002

Abstract

A computer-automated shape optimization methodology has been developed for the purpose of providing internal cooling systems designers the ability to optimize the internal cooling configuration, geometry and heat transfer enhancements for greater cooling efficiency and more durable turbine airfoils. The methodology presents the theory and practical programming requirements for coupling existing computer design and analysis tools together into a new and powerful design system. The goal of this paper is to demonstrate the computational advantages of using implicit sensitivity with the boundary element method (BEM) within this system over other more brute force methods. For this research, BEM algorithms for nonlinear heat conduction and thermo-elasticity were developed and coupled to an unstructured finite volume CFD code for the hot gas flow and a quasi-one-dimensional thermo-fluid system for the analysis of the internal coolant network. These computational tools were controlled by a constrained hybrid optimization algorithm to provide aerodynamic, thermal and internal fluid flow analyses on modified designs. The coolant supply total pressure, turbine inlet temperature, coolant wall thickness, thickness of ribs, rib positions, rib orientations, pin fin diameters and trip strip heights were incorporated into the set of optimization design variables. In order to improve performance, sensitivity gradients of the objective and constraint functions with respect to the geometric and heat transfer enhancement design variables were obtained using implicit differentiation of the boundary element system of equations. A three-to-one improvement in the optimization convergence rate and greater gradient accuracy were obtained for the two-dimensional thermal optimization problems. An order of magnitude larger computing time reduction was realized for three-dimensional thermal optimizations at the expense of additional memory, and another order of magnitude is expected for thermo-elastic optimization problems. Examples include studies of the accuracy of the design sensitivities with respect to forward and central finite differences, and validation of the optimization process using a symmetric cooled configuration.

Keywords: Design sensitivity; Thermo-structural optimization; Boundary elements

1. Introduction

The partial derivatives of the field variables (temperatures, temperature gradients, deformation, stress, etc.) and boundary values (heat fluxes, heat transfer coefficients, tractions, etc.) with respect to the set of design variables are very useful when performing a parametric study of a particular design. These partial derivatives are called design sensitivity coefficients. The implementation of gradient-based numerical optimization algorithms for inverse thermal shape design and optimization require these partial derivatives as part of their operation [1,2].

In general, there are four methods that can be used to determine sensitivity coefficients: (i) analytical differentiation, (ii) numerical differentiation of the solution by finite differences, (iii) direct implicit differentiation of the governing equations, and (iv) the adjoint variable method. In the arena of modern applied numerical methods, analytic differentiation of the governing equations is generally very difficult. The fourth method has been referred to as the adjoint variable method or the continuum approach. It uses variational concepts such as the material derivative [3]. By defining an adjoint problem, the sensitivity coefficients are found in terms of the primary and adjoint variables, thus requiring only the solution of one adjoint system to obtain

* Corresponding author. Tel.: +1-860-557-2585; fax: +1-860-557-2867.
E-mail addresses: martintj@pweb.com (T.J. Martin), dulikra@mae.uta.edu (G.S. Dulikravich).

[1] Tel.: +1-817-272-7376; fax: +1-817-272-5010.

0955-7997/03/$ - see front matter © 2003 Published by Elsevier Science Ltd.
doi:10.1016/S0955-7997(03)00056-0

the gradient with respect to every design variable. Although it has been proven successful with finite elements, the BEM version of the adjoint variable method was less satisfactory because the approximate adjoint tractions (or fluxes) could not be specified uniquely. The adjoint variable method requires a very complicated formulation of the optimization problem that needs to be developed uniquely for each objective function. Due to this fact, as well as its overall decreased accuracy versus discretized differentiation, only the second and third methods, finite differencing and implicit differentiation, will be discussed here.

The second method, finite differencing, is the simplest, most common and most computationally expensive strategy of obtaining sensitivity coefficients. It requires the brute force solution of the governing system discretized by the BEM once for every design variable when using first-order forward differencing formula.

$$\frac{\partial F}{\partial V_i} = \frac{F(V_i + \Delta V_i) - F(V_i)}{\Delta V_i} \quad (1)$$

If second-order accuracy is desired, the governing system must be evaluated twice per every design variable for central differencing. The finite differencing method for sensitivity calculations can be prohibitively expensive, especially when the design study or optimization concerns complex three-dimensional problems.

The third method involves the implicit differentiation of the equations at the system level [4]. Considerable effort has been applied to these techniques and they have been used extensively for the efficient implementation of shape optimization of large-scale structures. Implicit differentiation offers a practical design sensitivity calculation because the factorization of coefficient matrices needs to be performed only once and stored. In addition, they have been found to be more accurate than finite differences [5,6]. Kane and Saigal [7] obtained their sensitivity coefficients by the implicit differentiation of the coefficient matrices formed by the boundary integral equations of two-dimensional sub-structural problems. This method has been extended to three-dimensional elasticity problems [8].

2. Heat conduction using the BEM

The BEM is used to find the heat conduction field inside internally cooled turbine blades with a thermal barrier coating. The conduction of heat within the solid turbine blade was modeled by the following steady-state non-linear partial differential equation:

$$\nabla \cdot (k_m(T)\nabla T) = 0 \quad (2)$$

Here, $k_m(T)$ is the temperature-dependent coefficient of thermal conductivity in the mth domain, and T is the temperature. This equation was subject to boundary conditions of $T = \bar{T}$ on Γ_1, $q = \bar{q}$ on Γ_2, and $-kq = h(T - T_{\mathrm{amb}})$ on Γ_3, where $q = \mathrm{d}T/\mathrm{d}n$, n is the direction normal to the boundary Γ, h is the heat transfer coefficient and T_{amb} is the ambient or bulk temperature. The computational domain was divided into a finite number of sub-domains where the material properties within each sub-domain varied continuously, homogeneously and isotropically. The steady-state heat conduction Eq. (1) was numerically evaluated with the Boundary Element Method (BEM) [9], which is written in boundary integral form as follows:

$$c(x)T(x) + \int_\Gamma q^*(x,\xi)T(\xi)\mathrm{d}\Gamma = \int_\Gamma u^*(x,\xi)q(\xi)\mathrm{d}\Gamma \quad (2a)$$

Here, u^* is the fundamental solution, $q^* = \partial u^*/\partial n$, x is the coordinate of the source point, and $\mathrm{d}\Gamma$ is the boundary contour following coordinate.

The boundaries were discretized with N_{BE} linear isoparametric boundary elements connected at their end-points between N_{BN} boundary nodes. Typically, a two-dimensional section of a cooled turbine blade was discretized with approximately 300 boundary elements, enough to capture the details of the internal cooling scheme, rib fillets, pin fins and impingement holes. The three-dimensional boundary element meshes were quite large, having about 1500 boundary elements, although not as refined as compared to the two-dimensional cases. The boundary elements were numerically integrated using Gaussian quadrature, and a self-adaptive cubic coordinate transformation was used for the singular and near singular boundary elements [10]. For three-dimensional problems, the integration of singular boundary elements was accomplished by transforming each quadrilateral into two triangles with the singular pole at one vertex [11]. The resulting system of equations was expressed in matrix form with $\{\mathbf{T}\}$ and $\{\mathbf{Q}\}$ being the vectors of nodal temperatures and fluxes as follows:

$$[\mathbf{H}]\{\mathbf{T}\} = [\mathbf{G}]\{\mathbf{Q}\} \quad (3)$$

The results of the two-dimensional and three-dimensional BEM were compared to other analysis programs, such as ANSYS, and to experimental data for convectively cooled turbine blades and very good agreement was demonstrated [12]. The BEM required a large amount of computer storage for realistic turbine airfoils because the entire coefficient matrices $[\mathbf{H}]$ and $[\mathbf{G}]$, as well as the inverted solution matrix, were stored. Without the use of implicit differentiation, BEM heat conduction required about 300 MB, and this amount was doubled when implicit differentiation was used.

3. Conjugate heat transfer

The turbulent thermo-viscous aerodynamic flow field in the turbine cascade was coupled to the heat conduction in the adjacent solid material of the blade by using an iterative application of compatibility boundary conditions

[13]. The conjugate heat transfer analysis was started with a CFD analysis of the turbine cascade using an unstructured compressible turbulent Navier–Stokes solver [14] and given an initial guess to the outer airfoil wall temperature, T_o. Once converged, the flow-field analysis code computed turbulent heat fluxes, Q_o, that were applied as heat flux boundary conditions directly to the BEM heat conduction analysis code. These heat fluxes were relaxed with a relaxation factor of 0.5, starting from the adiabatic condition. After converging on the non-linear boundary conditions of the coolant passages, new outer (hot) wall temperatures were computed by the BEM. Since this wall temperature variation was, in general, different from the wall temperatures specified to the hot gas flow-field analysis code, the new variation was applied as a boundary condition again to the CFD code. The new CFD solution then returns heat fluxes that were again different from the ones that were used initially. This process was repeated several times until the heat fluxes converged. Thereafter, heat transfer coefficients on the outer turbine airfoil boundary, h_o, were computed from the converged hot surface temperatures and fluxes and the corresponding turbine inlet temperature, $h_o = Q_o/(T_o - T_{\text{inlet}})$.

The heat transfer on the walls of the coolant passages was coupled to a system of equations that modeled the quasi-one-dimensional flow in the coolant network with centrifugal pumping. In that program, the finite element method was used for a system of fluid elements (segments) and solved for the unknown total pressure, total temperature and flow rate in the coolant flow passages. The Newton–Raphson iteration method was used to converge the system of equations. Forced convection correlations for walls with ribbed turbulators, banks of pin fins and impingement jets were used to obtain heat transfer coefficients and friction factors. The integrated heat flux through the coolant wall boundary elements were applied as boundary conditions to the thermal-fluid system of the internal coolant flow. Since the coolant walls heat up the coolant air, the bulk temperatures of the coolant air are heat flux-dependent, which subsequently change the heat conduction in the metal. Therefore, the thermal-fluid system was included in the conjugate heat transfer loop. This iteration was found to be necessary for an accurate prediction of the temperature in the metal. The conjugate procedure required only a small number of iterations (3–9) between the three programs.

4. Implicit differentiation for thermal design sensitivity coefficients

The system of boundary integral equations was differentiated with respect to the vector of design variables, V_i, as follows:

$$\begin{aligned}
&\frac{\partial c(x)}{\partial V_i}T(x) + c(x)\frac{\partial T(x)}{\partial V_i} + \int_\Gamma \frac{\partial q^*(x,\xi)}{\partial V_i}T(\xi)\mathrm{d}\Gamma \\
&\quad + \int_\Gamma q^*(x,\xi)\frac{\partial T(\xi)}{\partial V_i}\mathrm{d}\Gamma + \int_\Gamma q^*(x,\xi)T(\xi)\frac{\partial\,\mathrm{d}\Gamma}{\partial V_i} \\
&\quad = \int_\Gamma \frac{\partial u^*(x,\xi)}{\partial V_i}q(\xi)\mathrm{d}\Gamma + \int_\Gamma u^*(x,\xi)\frac{\partial q(\xi)}{\partial V_i}\mathrm{d}\Gamma \\
&\qquad + \int_\Gamma u^*(x,\xi)q(\xi)\frac{\partial\,\mathrm{d}\Gamma}{\partial V_i}
\end{aligned} \tag{4}$$

The derivatives of the boundary conditions were found in the same way, namely:

$$\text{Dirichlet}: \quad \frac{\partial \bar{T}}{\partial V_i} = 0 \tag{5}$$

$$\text{Neumann}: \quad \frac{\partial \bar{q}}{\partial V_i} = 0 \tag{6}$$

Robin :

$$\begin{aligned}
&-k\frac{\partial q}{\partial V_i} - \frac{\partial k(T)}{\partial T}\frac{\partial T}{\partial V_i}q \\
&\quad = \frac{\partial h}{\partial V_i}(T - T_{\text{amb}}) + h\left(\frac{\partial T}{\partial V_i} - \frac{\partial T_{\text{amb}}}{\partial V_i}\right)
\end{aligned} \tag{7}$$

After discretization but before the application of boundary conditions, the linear algebraic system can be expressed in the following form:

$$\begin{aligned}
&[\partial\mathbf{H}/\partial\mathbf{V}]\{\mathbf{T}\} + [\mathbf{H}]\{\partial\mathbf{T}/\partial\mathbf{V}\} \\
&\quad = [\partial\mathbf{G}/\partial\mathbf{V}]\{\mathbf{Q}\} + [\mathbf{G}]\{\partial\mathbf{Q}/\partial\mathbf{V}\}
\end{aligned} \tag{8}$$

There are two possible ways of determining the differentiated coefficient matrices, [**C**], [**G**], and [**H**]. In most BEM implicit differentiation methodologies, the derivatives of the fundamental solution that appear in the preceding equation are calculated implicitly from the spatial derivative in the $\vec{x}$ and $\vec{\xi}$ coordinate systems [8], namely:

$$\frac{\partial u^*}{\partial V_i} = \frac{\partial u^*}{\partial x_m}\left(\frac{\partial x_m}{\partial V_i} - \frac{\partial \xi_m}{\partial V_i}\right) \tag{9}$$

Unfortunately, these integrands result in singular fundamental solutions of the order $1/r$ and $1/r^2$ in two-dimensional problems, and $1/r^2$ and $1/r^3$ in three-dimensional problems, resulting in the need for hyper-singular integration. The rigid body assumption can be used to compute some weakly singular integrals that occur when the source and field points coincide but, in general, special methods are needed. Hyper-singular integration techniques are somewhat complex, requiring Laurent series expansions of the hyper-singular integrand about the singular point and a transformation to a local polar coordinate system in three-dimensional problems [15,16]. Although hyper-singular integration is complex and time-consuming, the savings is realized because the numerical integration of the differentiated fundamental solutions needs to be performed only twice for two-dimensional problems and three times for three-dimensional problems. Finite differencing of the boundary contours or surfaces, $\partial x_m/\partial V_i$, would still be necessary if the design variables could not be expressed as closed form functions of the boundary contour or surface.

Implicit differentiation of the fundamental solution has been avoided for a slightly more expensive method of finite differencing the coefficient matrices [d**C**/d**V**], [d**H**/d**V**] and [d**G**/d**V**], namely:

$$\left[\frac{\partial \mathbf{H}}{\partial V_i}\right] = \frac{[\mathbf{H}(V_i + \Delta V_i)] - [\mathbf{H}(V_i)]}{\Delta V_i} \tag{10}$$

The boundary needs to be integrated once for every design variable perturbation. Its only advantage over implicit differentiation is that it was very easy to program, particularly because it did not require the implementation of hyper-singular integration. Since most CPU time is involved in the factorization of the coefficient matrix [**A**], rather than during the integration over the boundary, this method still provided a substantial reduction in computational time at the expense of the memory required to store two sets of BEM coefficient matrices. The linear system of equations can then be solved for the unknown derivatives of temperature and flux $\partial T/\partial V_i$ and $\partial q/\partial V_i$. The inversion of the coefficient matrix [**A**] has not changed from the heat conduction analysis of the original design and is given by:

$$[\mathbf{A}]^{-1}\left\{\frac{\partial \mathbf{X}}{\partial V_i}\right\} = -[\mathbf{C}'][\mathbf{T}\} - [\mathbf{H}']\{\mathbf{T}\} + [\mathbf{G}']\{\mathbf{Q}\} + \left\{\frac{\partial \mathbf{F}}{\partial V_i}\right\} \tag{11}$$

5. Gradients of the thermal objective functions

The gradient of each of the three thermal objective functions has been computed given the thermal sensitivity coefficients of $\partial T/\partial V_i$ and $\partial q/\partial V_i$. These quantities are then used in the differentiated objective function. The gradient of the integrated temperature objective appears as follows, including the differentiation of the boundary Jacobian, $|\vec{\eta}|$, with respect to the design variable vector, V_i.

$$\frac{\partial F(V_i)}{\partial V} = \int_\Gamma 2(T-\bar{T})\left(\frac{\partial T}{\partial V_i} - \frac{\partial \bar{T}}{\partial V_i}\right)\mathrm{d}\Gamma + \int_\Gamma (T-\bar{T})^2 \frac{\partial|\vec{\eta}|}{\partial V_i}\mathrm{d}\xi \tag{12}$$

When the mean temperature is used rather than the target temperature, the implicitly differentiated mean temperature has its own sensitivity

$$\frac{\partial \bar{T}}{\partial V_i} = \frac{\int_\Gamma \frac{\partial T}{\partial V_i}\mathrm{d}\Gamma + \int_\Gamma T\frac{\partial|\vec{\eta}|}{\partial V_i}\mathrm{d}\xi}{\int_\Gamma \mathrm{d}\Gamma} - \bar{T}\frac{\int_\Gamma \frac{\partial|\vec{\eta}|}{\partial V_i}\mathrm{d}\xi}{\int_\Gamma \mathrm{d}\Gamma} \tag{13}$$

The gradient of the net heat flux objective has also been derived for temperature-dependent thermal conductivity. The implicit differentiation requires the use of BEM design sensitivities of the flux as well as of the temperature when the thermal conductivity is temperature-dependent.

$$\begin{aligned}\frac{\partial F(V_i)}{\partial V_i} &= -\int_{\Gamma_0} \frac{\partial Q}{\partial V_i}\mathrm{d}\Gamma \\ &= \int_{\Gamma_0} k\frac{\partial(\partial T/\partial n)}{\partial V_i}\mathrm{d}\Gamma + \int_{\Gamma_0} \frac{\mathrm{d}k}{\mathrm{d}T}\frac{\partial T}{\partial V_i}\frac{\partial T}{\partial n}\mathrm{d}\Gamma \\ &\quad + \int_{\Gamma_0} k\frac{\partial T}{\partial n}\frac{\partial|\vec{\eta}|}{\partial V_i}\mathrm{d}\xi\end{aligned} \tag{14}$$

6. Gradients of the thermal constraint functions

Greater potential savings of computational resources can be achieved with the use of implicit differentiation for the computation of gradients of the constraint functions. For thermally-constrained shape optimization problem, the temperature field needs to be computed in order to determine the maximum temperature. Therefore, a BEM solution of the non-linear heat conduction equation is required for every constraint function analysis, just as for the thermal objective function analysis. When the constraints are active or violated, the gradient of the constraint function with respect to the design variables is needed in order to project the searching directions. These gradient calculations are needed more often for the gradient-based constraint restoration sub-optimization procedure that restores infeasible designs back to the feasible region.

A finite differencing gradient computation can be costly, requiring at least one heat conduction analysis per design variable. But implicit differentiation of the constraint function can yield substantial savings because of the ability to re-use the previous inversion of the BEM coefficient matrix, $[\mathbf{A}]^{-1}$. The implicitly differentiated inequality and equality constraint function has the following form:

$$\frac{\partial h(V_i)}{\partial V_i} = \frac{1}{\bar{T}_{\max}}\left.\frac{\partial T}{\partial V_i}\right|_{T_{\max}} \tag{15}$$

7. Comparison of finite differencing to implicit differentiation

In order to improve performance, sensitivity gradients of the objective and constraint functions with respect to the geometric and boundary condition design variables were obtained using implicit differentiation of the boundary element system of equations. The accuracy of the design sensitivity was studied with respect to forward and central finite differences over a range of differencing stepsizes. We have found that there is a trade-off between truncation errors and round-off errors that is dependent upon the type of design variable. Truncation errors are larger with bigger differencing stepsizes, but round-off errors are larger with smaller step sizes.

Gradients of the uniform temperature objective function (Eq. (12)), and maximum temperature constraint function (Eq. (15)), were determined on the initial guess of the Rankine oval constrained conjugate optimization problem. The gradients were obtained over a range of finite differencing stepsizes. These stepsizes were given with respect to the base stepsizes presented in Table 1. These base stepsizes were those that were manually chosen and used in the previous Rankine oval optimization example. The Rankine oval chord was 0.2 m. Table 1 also lists the design variable bounds, $V_{\min}$ and $V_{\max}$, and the gradient is non-dimensionalized by $(V_{\min}-V_{\max})$. The trade-off between truncation and round-off error is apparent in Fig. 1. Notice that the derivative of the uniform temperature objective function is accurate over a wide range of differencing stepsizes. As the stepsize becomes bigger, the truncation error dominates. The implicit derivative is as accurate as the central-difference derivative.

Geometry parametric variables have larger round-off errors than do the beta-spline vertices or the boundary condition variables (Fig. 2). The derivative of the thermal objective function with respect to the strut centerline coordinate has round-off errors that are dominant in stepsizes below 10^{-1} of the base perturbation. The central differenced derivative coincides with the implicit derivative between 10^{-1} and 10^{1}, while the forward explicit differenced derivative is invalid below the base stepsize. Similar behavior was apparent for the strut thickness variable shown in Fig. 3.

The boundary condition design variables were less sensitive to round-off errors than the geometry parameters, but the implicit derivatives tended to have a slight bias caused by the non-linearity of the boundary condition.

Table 1
Perturbation step sizes used for comparing design sensitivities using explicit finite differencing and implicit differentiation for the symmetric airfoil case

Design variable	Base stepsize	Design variable range
β-Spline vertex	0.001 × chord	0.1–5.0 mm
Strut centerline coordinate	0.001 × chord	Dependent (± 5 mm)
Strut thickness	0.001 × chord	Dependent (0–5 mm)
Wall roughness	0.001 mm	0.0–0.05 × cavity height
Coolant mass flow rate	0.0001 kg/s	0.005–0.05 kg/s
Turbine inlet temperature	1 K	1000–2000 K

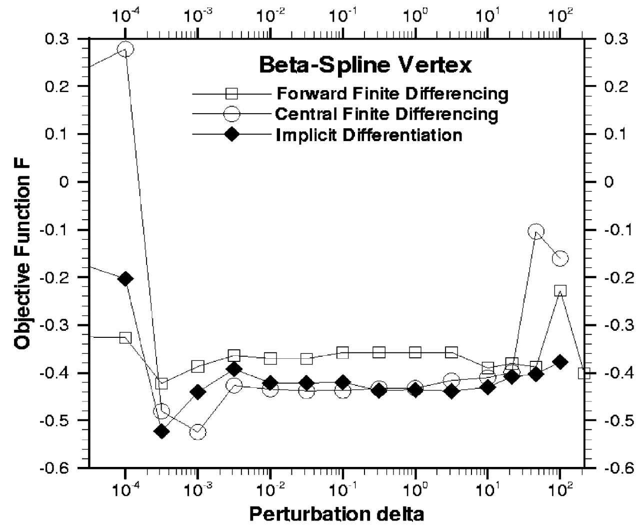

Fig. 1. Finite differenced and implicitly differentiated uniform temperature objective function with respect to beta spline vertices.

The examples of these types of derivatives with respect to the wall roughness, coolant mass flow rate, and turbine inlet temperature design variables are demonstrated in Figs. 4–6, respectively.

The implicit BEM system was linearized and solved non-iteratively for the derivatives of temperature and heat flux, but the bulk coolant temperatures were actually a non-linear function of the heat flux. The bias is especially evident in the turbine inlet temperature because the heat flux is a strong function of that variable. The implicit system was solved for the heat flux derivatives using a guess to the heat flux in the quasi-one-dimensional coolant network solver. That guessed heat flux was taken from the conjugate solution of the unperturbed coolant configuration. Incorporating the heat flux non-linearity in the implicit BEM system could probably alleviate the bias.

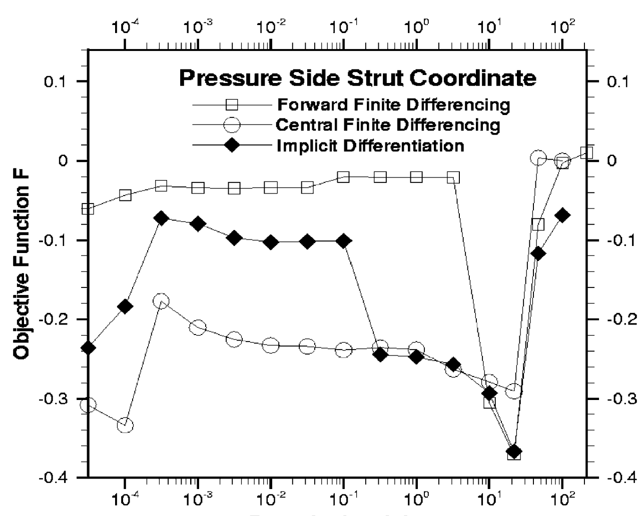

Fig. 2. Finite differenced and implicitly differentiated uniform temperature objective function with respect to strut coordinates.

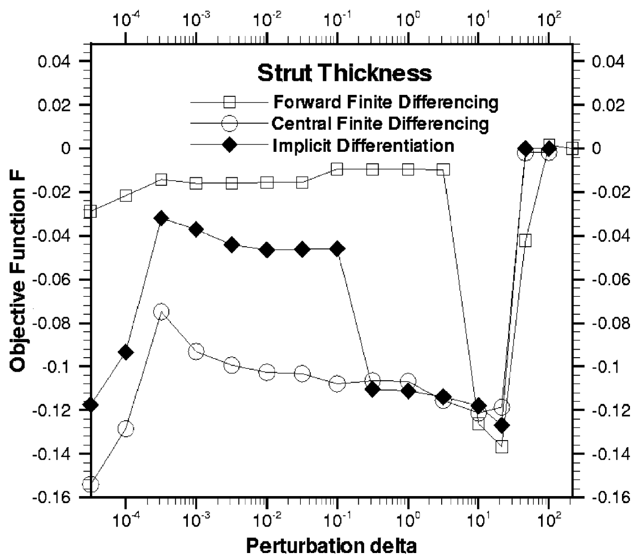

Fig. 3. Finite differenced and implicitly differentiated uniform temperature objective function with respect to strut thickness.

A comparison between computing time from the explicit finite differenced and implicit differentiated design sensitivities is shown in Fig. 7. In this example, a symmetric internally cooled airfoil was optimized in order to produce a more uniform temperature field in the metal with the maximum temperature constrained [1]. Each circle or square depicts one unconstrained optimization cycle. In order to determine if the converged solution was optimal, the optimization was started from several different initial guess designs, and the final design was deemed optimal (from the perspective of the objective that was set to it) because each optimization achieved the same final result.

These results have shown that two-dimensional constrained optimization problems can be solved in one-third of the computing time when using implicit differentiation over

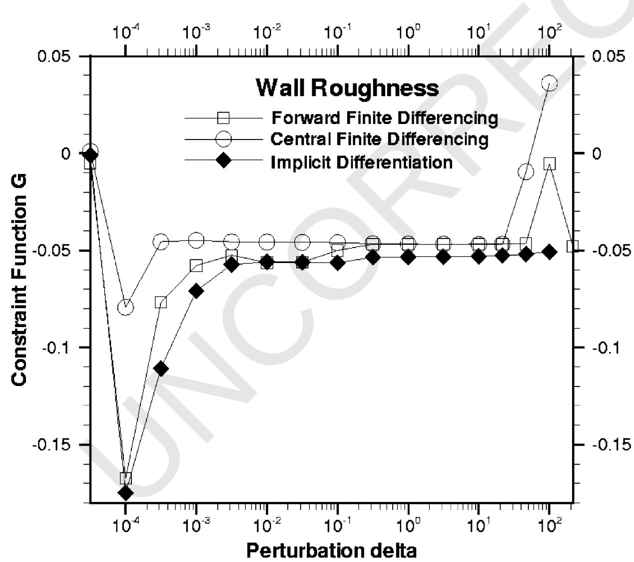

Fig. 4. Finite differenced and implicitly differentiated maximum temperature constraint with respect to coolant passage wall roughness.

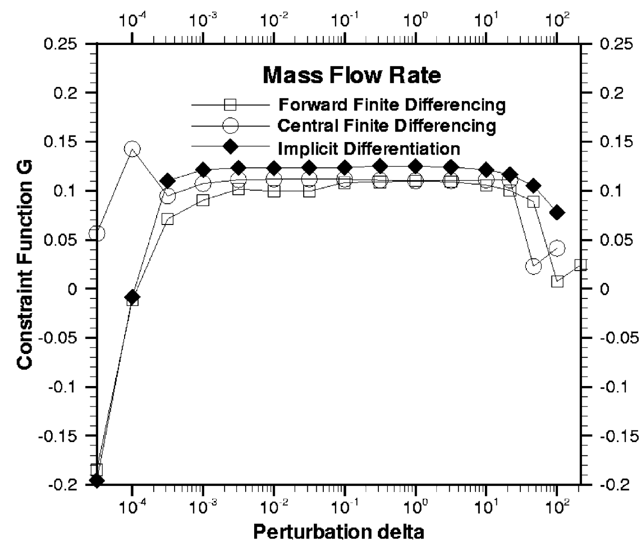

Fig. 5. Finite differenced and implicit differentiated maximum temperature constraint function with respect to coolant flow rate.

explicit finite differencing to obtain design sensitivities. Estimates of three-dimensional thermally constrained problems have demonstrated a ten-fold advantage in the computing time. Preliminary estimates of the thermo-elastically constrained problem have indicated the savings in the computing time to be about thirty-fold.

8. Thermo-elasticity

This research effort continued with the integration of a static thermo-elastic solver using the BEM. The resulting thermal loads in the turbine blade predicted by the aero-thermal program were submitted to the thermo-elastic solver for a development of the deformation and stress fields in the turbine blade. This inter-disciplinary coupling

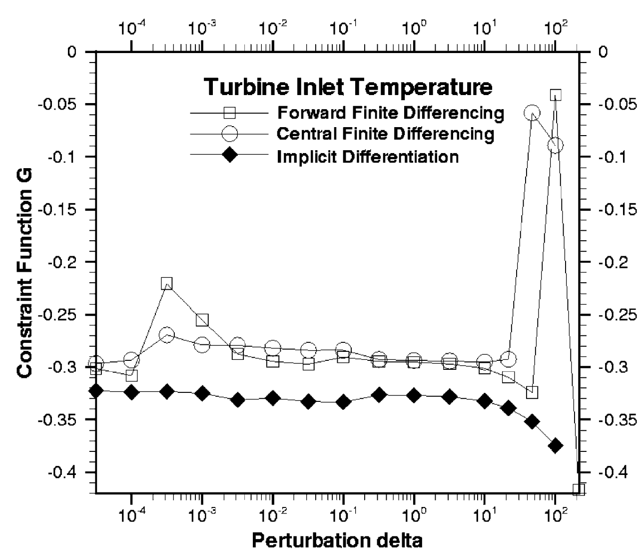

Fig. 6. Finite differenced and implicit differentiated maximum temperature constraint function with respect to turbine inlet temperature.

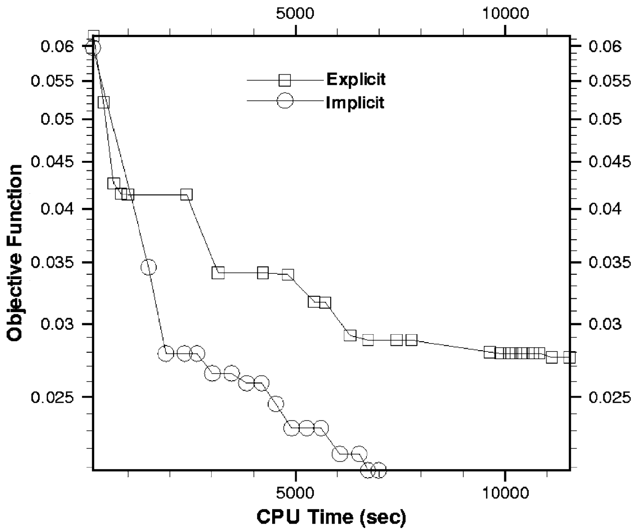

Fig. 7. Convergence history of uniform temperature objective function during optimization of an internally cooled turbine airfoil.

provides a turbine designer with a tool to confidently expand the limits and improve performance of the internal cooling scheme.

The governing partial differential equations of elastostatics assume that there is a linear relationship between the stress and the strain response. It also neglects any changes in the orientation of the body due to displacements. The two-dimensional state of stress at a point is defined using a second order symmetric stress tensor σ_{ij}. These stress components must satisfy the following equilibrium equations throughout the interior of the solid body,

$$\frac{\partial \sigma_{ij}}{\partial x_j} + b_k = 0 \tag{16}$$

where b_k are the net body forces per unit volume necessary to keep the body in equilibrium. Equilibrium on the boundary requires that $p_k = \sigma_{kj} n_j$, where n_k is the unit outward normal vector to the surface Γ. The state of strain at a point within a solid object is denoted by the second order symmetric strain tensor, ϵ_{kj}. The states of stress and strain for an isotropic solid body are related through the stress–strain relations, also known as Hooke's Law, which depend on the material behavior. Thermo-elastic effects, which involve dilatation or contraction due to changes in temperature, can be included as initial stresses, σ_{ij}^0. The initial stresses for a thermally isotropic material can be added to the stress–strain relation, that is,

$$\sigma_{ij} = \lambda \delta_{ij} \frac{\partial u_k}{\partial x_k} + \mu \left(\frac{\partial u_i}{\partial x_j} + \frac{\partial u_j}{\partial x_i} \right) - \lambda \beta (T - T_0) \delta_{ij} \tag{17}$$

Here, u_k is the vector displacement field, δ_{ij} is the Kronecker delta symbol, μ is the shear modulus, λ is Lame's constant, β is the thermal expansion coefficient, T is the temperature, and T_0 is the reference temperature.

The BEM has been found to be an effective solution strategy of the Navier–Cauchy equation and thermo-elasticity [17]. The initial stress term can be used to deal with thermal expansion and other non-linear effects such as plasticity [18]. The result is the boundary/domain integral equation for static thermo-elasticity problems with body forces. In this equation, the initial stress field and body forces remain as domain integrals, and we obtain:

$$c_{\ell k}(\vec{x}) u_k(\vec{x}) + \int_\Gamma p^*_{\ell k} u_k \, d\Gamma = \int_\Gamma u^*_{\ell k} p_k \, d\Gamma + \int_\Omega u^*_{\ell k} b_k \, d\Omega - \int_\Omega \epsilon^*_{\ell jk} \lambda \beta (T - T_0) \delta_{jk} \, d\Omega \tag{18}$$

In order to avoid the need for an internal mesh, and to preserve the boundary-only nature of the BEM, the domain integrals can be transformed into boundary (surface) integrals. The first implementation of the use of the divergence theorem to transform body-loading effects into boundary integrals was presented by Cruse [19]. Rizzo and Shippy [17] presented a similar approach for thermo-elastic problems that could be easily adapted to gravitational and centrifugal loading by expressing the body forces as a differential of a scalar potential function $\nabla \psi = \vec{\Omega} \times (\vec{\Omega} \times \vec{R})$. The potential function satisfies the following harmonic relationship with Ψ_0 a constant defined by $\nabla^2 \psi = \Psi_0$.

The body force integral was integrated by parts and the divergence theorem was applied to transform one domain integral to a boundary integral [18]. After applying the definition of the Galerkin vector, the following expression was obtained for the body force integral:

$$\int_\Omega u^*_{\ell k} b_k \, d\Omega = \int_\Gamma U^*_{n\ell} \psi \, d\Gamma + \frac{1 - 2\nu}{2(1 - \nu)} \left\{ \int_\Gamma U^*_\ell \frac{\partial \psi}{\partial n} d\Gamma - \int_\Gamma P^*_\ell \psi \, d\Gamma - \Psi_0 \int_\Gamma G^*_{n\ell} \, d\Gamma \right\} \tag{19}$$

The thermo-elastic effects can be presented in a similar fashion. The initial stress term is equivalent to adding a body force equal to $(-\gamma \partial (T - T_0)/\partial x_k)$. The Galerkin fundamental solution is differentiated three times. The resulting thermo-elastic kernels are identical the body force boundary kernels, namely:

$$\int_\Omega \epsilon^*_{\ell jk} \lambda \beta (T - T_0) \delta_{jk} \, d\Omega = \frac{(1 - 2\nu)\gamma}{2(1 - \nu)} \left\{ \int_\Gamma P^*_\ell (T - T_0) d\Gamma - \int_\Gamma U^*_\ell \frac{\partial T}{\partial n} d\Gamma \right\} \tag{20}$$

where ν is the Poisson's ratio. After the application of boundary element discretization and numerical integration of the integrands, the BEM system of equations for thermo-elasticity can be written in matrix form as follows:

$$[\mathbf{H}_E]\{\mathbf{U}\} = [\mathbf{G}_E]\{\mathbf{P}\} + [\mathbf{D}_n]\{\Psi\} + \frac{1 - 2\nu}{2(1 - \nu)} \left\{ [\mathbf{G}_g] \left\{ \frac{\partial \Psi}{\partial n} - \gamma \mathbf{Q} \right\} - [\mathbf{H}_h]\{\Psi - \gamma(\mathbf{T} - T_0)\} - [\mathbf{E}_n]\Psi_0 \right\} \tag{21}$$

The vectors $\{\mathbf{U}\}$ and $\{\mathbf{P}\}$ represent the values of the displacements and tractions at the boundary nodal locations. The centrifugal potential function, $\{\Psi\}$, temperatures, $\{\mathbf{T}\}$, and boundary heat fluxes, $\{\mathbf{Q}\}$, are known, and can be multiplied by their respective coefficient matrices. The application of boundary conditions allows the columns of the $[\mathbf{H}_\mathrm{E}]$ and $[\mathbf{G}_\mathrm{E}]$ matrices to be multiplied by the known displacements and tractions, while the unknowns are passed into a vector $\{\mathbf{X}\}$. The result is a system of equations, $[\mathbf{A}]\{\mathbf{X}\} = \{\mathbf{F}\}$, that can be solved by inverting the coefficient matrix $[\mathbf{A}]$ with Gaussian elimination, LU decomposition, or Singular Value Decomposition (SVD) [20]. The latter solver is necessary for turbine blades with extremely thin coolant walls and thermal barrier coatings that create ill-conditioned matrices.

9. Implicit differentiation for thermo-elastic design sensitivities

A new formulation for structural design sensitivity was developed for elastic solids to consistently account for the effects of thermal expansion along with centrifugal loading. Implicit differentiation of the governing system was shown to be capable of generating accurate sensitivities without the need for domain integration [21]. The discretized form of the boundary integral equation for thermo-elasticity with centrifugal body forces was differentiated with respect to the set of design variables, V_i, as follows:

$$
\begin{aligned}
&[\partial\mathbf{H}/\partial V]\{\mathbf{U}\} + [\mathbf{H}]\{\partial\mathbf{U}/\partial V\} = \\
&\quad [\partial\mathbf{G}/\partial V]\{\mathbf{P}\} + [\mathbf{G}]\{\partial\mathbf{P}/\partial V\} \\
&\quad + [\partial\mathbf{D}_n/\partial V]\{\Psi\} + \frac{1-2\nu}{2(1-\nu)}\left\{[\partial\mathbf{G}_g/\partial\mathbf{V}]\left\{\frac{\partial\Psi}{\partial n} - \gamma\mathbf{Q}\right\}\right. \\
&\quad -[\mathbf{G}_g]\{\gamma\partial\mathbf{Q}/\partial\mathbf{V}\} - [\partial\mathbf{H}_h/\partial\mathbf{V}]\{\Psi - \gamma(\mathbf{T} - T_0)\} \\
&\quad \left. +[\mathbf{H}_h]\{\gamma\partial\mathbf{T}/\partial\mathbf{V}\} - [\partial\mathbf{E}_n/\partial\mathbf{V}]\Psi_0\right\} \qquad (22)
\end{aligned}
$$

Since the centrifugal body force field is not a function of the design variables, the sensitivity of the centrifugal potential function is neglected, i.e. $\partial\Psi/\partial\mathbf{V} = 0$. The design sensitivities of the temperature, T, and flux, q, do affect this equation.

This sensitivity equation can be solved for the unknown displacement and traction sensitivities on the boundary given the boundary conditions $\partial\bar{\mathbf{U}}/\partial V = 0$ and $\partial\bar{\mathbf{P}}/\partial V = 0$ where $\bar{\mathbf{U}}$ and $\bar{\mathbf{P}}$ were specified on the direct problem. The advantage is that the BEM coefficient matrix factorization can be saved and re-used in the design sensitivity analysis. This factorization process (using either a standard LU decomposition or SVD) is generally the most computationally demanding part of the overall boundary element analysis. This is especially true for three-dimensional turbine blades because of the very large dense matrices to factor and because the SVD solver is usually needed since the matrix is ill conditioned due to the thin turbine blade walls and coating. Another source of savings is that the boundary stress sensitivities can be obtained without the need for additional integration or matrix factorization.

10. Conclusions

The design and optimization system that was presented here combines parametric modeling of the internal geometry, and computational aerodynamics, thermodynamics, and structural analysis programs into a fully computer-automated design tool for the optimization of internally cooled turbine blades with thermal barrier coatings. A hybrid optimization algorithm controlled these analysis programs in order to minimize an aero-thermal optimization objective function subject to one or more thermal and structural constraint functions. The purpose of this paper was to demonstrate the improved performance and accuracy that can be achieved when one uses implicit differentiation of the governing heat conduction and thermo-elasticity systems of equations in order to obtain sensitivities of these solutions to the optimization design variables. Results have shown that the optimization convergence rate can be reduced by a factor of three for two-dimensional problems, and much greater savings for three-dimensional problems, as well as an improvement in the accuracy of the design sensitivities.

Since its original conception at the Department of Aerospace Engineering at the Pennsylvania State University, this multi-disciplinary design, analysis and optimization tool has since been further developed, adapted and improved by the Turbine Durability and Systems Optimization Group at the Pratt and Whitney Aircraft Company. This system has been applied to real and much more complex cooled turbine blades and vanes, including those with film cooling. The system has undergone extensive validation efforts and the conjugate heat transfer results have compared very well to experimental data and to results from other analysis systems. Ultimately, the resulting thermal loads in the turbine blade and the effects of the thermo-elastic deformation were built into the design process, providing a turbine designer with a tool to confidently push the limits, durability and performance of the cooled turbines [22].

References

[1] Martin TJ, Dulikravich GS. Aero-thermo-elastic concurrent design optimization of internally cooled turbine blades. In: Kassab AJ, Aliabadi MH, editors. Coupled Field Problems. Series on Advances in Boundary Elements, Boston, MA: WIT Press; 2001. p. 137–84. chapter 5.

[2] Dulikravich GS, Martin TJ, Dennis BH, Foster NF. Multidisciplinary hybrid constrained ga optimization. In: Miettinen K, Makela MM, Neittaanmaki P, Periaux J, editors. EUROGEN'99—Evolutionary algorithms in engineering and computer science. Recent advances and industrial applications, Jyvaskyla, Finland: Wiley; 1999. p. 231–60. May 30–June 3; chapter 12.

[3] Meric RA. Differential and integral sensitivity formulations and shape optimization by BEM. Engng Anal Bound Elem 1995;15:181–8.

[4] Hafka RT, Malkus DS. Calculation of sensitivity derivatives in thermal problems by finite differences. Int J Numer Meth Engng 1981; 17:1811–21.

[5] Aliabadi MH, Mellings SC. Boundary element formulations for sensitivity analysis and crack identification. In: Ingham DB, Wrobel LC, editors. Boundary integral formulations for inverse analysis. Computational Mechanics Publications; 1997.

[6] Kane JH, Zhao G, Wang H, Guru Prasad K. Boundary formulations for three-dimensional continuum structural shape sensitivity analysis. J Appl Mech 1992;59:827–34.

[7] Kane JH, Saigal S. Design sensitivity analysis of solids using BEM. J Engng Mech, ASCE 1998;114(10):1703–22.

[8] Yamakazi K, Sakamoto J, Kitano M. Three-dimensional shape optimization using the boundary element method. AIAA J 1994;32(6).

[9] Brebbia CA. The boundary element method for engineers. New York: Wiley; 1978.

[10] Telles JCF. A self-adaptive coordinate transformation for efficient numerical evaluation of general boundary element integrals. Int J Numer Meth Engng 1987;24:959–73.

[11] Aliabadi MH, Hall WS. The regularizing transformation integration method for boundary element kernels, comparison with series expansion and weighted Gaussian integration methods. Engng Anal Bound Elem 1989;6(2).

[12] Martin TJ. Computer-automated multi-disciplinary analysis and design optimization of internally cooled turbine blades. PhD Dissertation. Department of Aerospace Engineering, The Pennsylvania State University; 2001

[13] He M, Kassab AJ, Bishop AJ, Minardi A. An iterative FDM/BEM method for the conjugate heat transfer problem—parallel plate channel with constant outside temperature. Engng Anal Bound Elem 1995;15:43–50.

[14] Han Z-X, Dulikravich GS, Dennis BH. Simultaneous prediction of external flow-field and temperature in internally cooled 3-D turbine blade material. Int J Turbo Jet-Engines 2001;18(1):47–58.

[15] Mikhilin SC. Multidimensional singular integral equations. London: Pergamon Press; 1965.

[16] Guiggiani M, Krishnasamy G, Rudolphi TJ, Rizzo FJ. A general algorithm for the numerical solution of hyper-singular boundary element integral equations. ASME J Appl Mech 1992;59:604–14.

[17] Rizzo FJ, Shippy DJ. An advanced boundary integral equation method for three-dimensional thermo-elasticity. Int J Numer Meth Engng 1977;11:1753–68.

[18] Brebbia CA, Dominguez J. Boundary elements, an introductory course. New York: McGraw-Hill; 1989.

[19] Cruse TA. Boundary integral equation method for three-dimensional elastic fracture mechanics analysis. Pratt and Whitney Aircraft Report AFOSR-TR-75-0813, 1975

[20] Press WH, Teukolsky SA, Vetterling WT, Flannery BP. Numerical recipes in FORTRAN, 2nd ed. The art of scientific computing, Cambridge: Cambridge University Press; 1986.

[21] Kane JH, Keshava-Kumar BL, Stabinsky M. Transient thermo-elasticity and other body force effects in boundary element shape sensitivity analysis. Int J Numer Meth Engng 1991;31:1203–30.

[22] Martin TJ, Dulikravich GS. Implicit BEM sensitivity for aero-thermo-structural optimization of coolant passages in turbine blades. AIAA paper 2002-5435, Ninth AIAA/ISSMO Multidisciplinary Analysis and Optimization Symposium, Atlanta, GA; September 4–6, 2002